Further Spectroscopy of the Diffuse Ionized Gas in NGC 891 and Evidence for a Secondary Source of Ionization

Richard J. Rand¹

Univ. of New Mexico, Dept. of Physics and Astronomy, 800 Yale Blvd, NE, Albuquerque, NM 87131

ABSTRACT

Two long-slit spectra of the diffuse ionized gas in NGC 891 are presented. The first reveals variations parallel to the major axis in emission line ratios in the halo gas at z=700 pc. It is found that filaments of H α emission show lower values of [N II]/H α , [S II]/H α and [O I]/H α . Although this result is expected if the filaments represent the walls of evacuated chimneys, it merely reflects a more general correlation of these ratios with H α surface brightness along the slit, and may simply arise from radiation dilution effects. Halo regions showing low line ratios are probably relatively close to ionizing sources in the disk below. The results highlight difficulties inherent in observations of edge-on galaxies caused by lack of knowledge of structure in the in-plane directions. The [S II]/[N II] ratio shows almost no dependence on distance along the major axis or H α surface brightness. Values of [O I]/H α indicate that H is 80–95% ionized (assuming $T=10^4$ K), with the higher ionization fractions correlating with higher surface brightness.

Much more interesting information on the nature of this gaseous halo comes from the second observation, which shows the vertical dependence of $[NII]/H\alpha$, $[SII]/H\alpha$, $[OI]/H\alpha$, and $[OIII]/H\beta$ through the brightest region of the DIG halo. The most surprising result, in complete contradiction to models in which the DIG is ionized by massive stars in the disk, is that $[O III]/H\beta$ rises with height above the plane for z > 1kpc (even as $[NII]/H\alpha$, $[SII]/H\alpha$, and $[OI]/H\alpha$ are rising, in line with expectations from such models). The run of [SII]/[NII] is also problematic, showing essentially no contrast with z. The [O III] emission probably arises from shocks, turbulent mixing layers, or some other secondary source of ionization. Composite models in which the line emission comes from a mix of photo-ionized gas and shocks or turbulent mixing layers are considered in diagnostic diagrams, with the result that many aspects of the data can be explained. Problems with the run of [SII]/[NII] still remain, however. There is a reasonably large parameter space allowed for the second component. For the photo-ionized component, only matter-bounded models succeed, putting a fairly strong restriction on the clumpiness of the halo gas. Given the many uncertainties, the composite models can do little more than demonstrate the feasibility of these processes

¹Visiting Astronomer, National Optical Astronomy Observatories, Tucson, AZ

as secondary sources of energy input. A fairly robust result, however, is that the fraction of H α emission arising from the second component probably increases with z. From values of [O I]/H α , H is essentially 100% ionized at z=0 kpc and 90% ionized at z=1 kpc (again assuming $T=10^4$ K).

Subject headings: galaxies: individual (NGC 891) – galaxies: ISM – galaxies: spiral – galaxies: structure – stars: formation

1. Introduction

The vast majority of the free electrons in the ISM of the Milky Way reside in a thick (\sim 900-pc scale height) diffuse layer known as the Reynolds layer or the Warm Ionized Medium (e.g. Reynolds 1993). This phase fills about 20% of the ISM volume, with a local midplane density of about 0.1 cm⁻³. Such a phase is now known to be a general feature of external star-forming galaxies, both spirals (e.g. Walterbos 1997; Rand 1996) and irregulars (e.g. Hunter & Gallagher 1990; Martin 1997, hereafter M97), where it is commonly referred to as Diffuse Ionized Gas (DIG). However, for edge-on spirals, only in the more actively star-forming galaxies does the gas manifest itself as a smooth, widespread layer of emission detectable *above* the HII region layer (Rand 1996). One such galaxy, NGC 891, is an attractive target for study, not only because of its prominent DIG layer (Rand, Kulkarni, & Hester 1990; Dettmar 1990), but also its proximity (D = 9.5 Mpc will be assumed here) and nearly fully edge-on aspect ($i > 88^{\circ}$; Swaters 1994).

One of the outstanding problems in the astrophysics of the ISM is the ionization of these layers. For the Reynolds layer, the local ionization requirement $(5 \times 10^6 \text{ s}^{-1} \text{ per cm}^2 \text{ of Galactic disk}$; Reynolds 1992) is comfortably exceeded (by a factor of 6 or 7) only by the ionizing output of massive stars. Alternatively, the ionization would require essentially all the power put out by supernovae (Reynolds 1984) – hence, this energy source could contribute at some level but probably cannot explain all of the diffuse emission. Photo-ionization models, on the other hand, must explain how the ionizing photons can travel ~ 1 kpc or more from their origin in the thin disk of massive stars to maintain this distended layer.

Crucial information on both the ionization and thermal balance of DIG comes from emission line ratios. In the Reynolds layer, ratios of [S II] $\lambda\lambda6716,6731$ and [N II] $\lambda\lambda6548,6583$ to H α are generally enhanced relative to their HII-region values, while [O III] $\lambda5007/\text{H}\alpha$ is much weaker. These contrasts are in accordance with models in which photons leak out of HII regions and ionize a larger volume, with the radiation field becoming increasingly diluted with distance from the HII region [Mathis 1986; Domgörgen, & Mathis 1994; Sokolowski 1994 (hereafter S94; see also Bland-Hawthorn, Freeman, & Quinn 1997)]. The effect of this dilution, measured by the ionization parameter, U, is primarily to allow species such as S and O, which are predominantly doubly ionized in HII regions, to recombine into a singly ionized state. The effect may be less noticeable

for N because it is mostly singly ionized in HII regions. The Wisconsin H α Mapper (WHAM) has been used to determine [O I]/H α in three low-latitude directions, resulting in values < 0.01 to 0.04 (Haffner & Reynolds 1997). Such low values imply, since the ionization of O and H are strongly coupled by a charge exchange reaction, that the diffuse gas is nearly completely ionized (Reynolds 1989).

Although weak, [O III] emission has been detected in two directions in the Reynolds layer at $b = 0^{\circ}$ (Reynolds 1985), with the result [O III]/H $\alpha = 0.06$. Reynolds postulated that the [O III] emission does not arise from diluted stellar ionization but from gas at about 10^{5} K, presumably the same gas as seen in C IV $\lambda 1550$ and O III] $\lambda 1663$ emission by Martin & Bowyer (1990). The origin of this rapidly cooling gas is unclear. [O III] emission from the DIG of NGC 891 and the implications for DIG ionization is one of the main subjects of this paper.

In external spiral galaxies, smooth increases in [S II]/H α and [N II]/H α vs. distance from HII regions have been observed in both the in-plane and vertical directions in accordance with photo-ionization models [Walterbos & Braun 1994; Dettmar & Schulz 1992; Rand 1997a (hereafter R97); Golla, Dettmar, & Domgörgen 1996; Greenawalt, Walterbos, & Braun 1997; Wang, Heckman, & Lehnert 1997]. The same trends are seen in irregulars (Hunter & Gallagher 1990; M97). This behavior has been revealed in NGC 891 through spectra using long slits oriented vertically to the plane. Dettmar & Schulz (1992) placed a slit at R = 65'' NE of the nucleus, while R97 took a deeper spectrum at R = 100'' NE. R97 found that [N II]/H α rises to a value of 1.4, implying a very hard ionizing spectrum. S94, which pays particular attention to modeling the DIG of NGC 891, can predict such a high value only by assuming a stellar IMF extending to 120 M $_{\odot}$, a reduction in cooling efficiency due to elemental depletions, and hardening of the radiation field by the intervening gas. [O I]/H α was not detected by Dettmar & Schulz (1992) in the halo of NGC 891 at R = 65'' NE, with an upper limit of 0.05. Dettmar (1992) also reported an upper limit on [O III]/H β of 0.4 at the same location.

A wealth of forbidden-line long-slit data on bright DIG and HII regions in irregular galaxies has recently been published by M97. Through the use of line-diagnostic diagrams (e.g. Baldwin, Phillips, & Terlevich 1981; Veilleux & Osterbrock 1987), she finds that while photo-ionization models can explain the line ratio behavior in many galaxies, the rather shallow fall-off of $[O\,III]/H\beta$ with distance from HII regions and the sharp rise in $[O\,I]/H\alpha$ seen in some galaxies imply a second source of ionization. Shocks are favored as the most likely second source.

The forbidden lines, though bright, are sensitive to metallicity and temperature and thus their interpretation in terms of ionization scenarios is complicated by uncertainties in abundances, degree of depletion, and sources of non-ionization heating. A more direct constraint on the ionizing spectrum has come from the very weak He I λ 5876 line. He I/H α is relatively easy to interpret in terms of the ratio of helium- to hydrogen-ionizing photons, allowing the hardness of the ionizing spectrum, the mean spectral type of the responsible stars, and the upper IMF cutoff to be inferred, assuming pure stellar photoionization. The results for the Reynolds layer (Reynolds & Tufte

1995), for HI worms from equivalent radio recombination lines (Heiles et al. 1996) and for NGC 891 (R97) all imply a much softer spectrum than do the forbidden lines. Further consequences of this discrepancy are discussed in the above three references.

The goal of this paper is to make further progress in understanding the ionization of DIG in spirals. The motivations are two-fold. First, the DIG halo of NGC 891 features several bright filaments and shells. It is likely that some of these are chimney walls (Norman & Ikeuchi 1989) surrounding regions of space evacuated by many supernovae. In this case, radiation from any continuing star formation near the base of the chimney will have an unimpeded journey to the walls, and thus the filaments may be directly ionized and show a spectrum more like an HII region than diffuse gas, which receives a significant contribution from relatively soft diffuse re-radiation (Norman 1991). If true, then the filaments should show lower [N II]/H α and [S II]/H α than the surrounding gas. To this end, a spectrum has been taken with a slit oriented parallel to the major axis, but offset into the halo gas, traversing several filaments.

The second purpose is to study in more detail the dependence of line ratios on z beyond the results reported in R97 for He I/H α and [N II]/H α . By adding measurements of [S II], [O III], [O I], and H β , one can form diagnostic diagrams and thus constrain the source(s) of ionization in the spirit of M97.

2. Observations

The spectra were obtained at the KPNO 4-m telescope on 1996 December 12–13. The slit positions are shown in Figure 1 (Plate 00) overlaid on the H α image of RKH and on a version of the image in which a median filter has been applied and the resulting smooth image subtracted to reveal the filaments clearly. Note also how the filaments connect onto the brightest HII regions in the disk, with few exceptions. For the first night, the slit was oriented parallel to the major axis and offset from it by 15" along the SE side of the minor axis. This slit position will be referred to as the "parallel slit." The slit position for the second night was the same as in R97's observations: oriented perpendicular to the major axis and centered R = 100" on the NW (approaching) side of NGC 891 – the "perpendicular slit." The slit length is 5', and the spatial scale is 0.69" per pixel.

The KPC-24 grating was used with the T2KB 2048x2048 CCD, providing a dispersion of 0.53Å per pixel, a resolution of 1.3Å, and a useful coverage of about 800 Å. For observations of red lines, the grating was tilted to give a central wavelength of about 6600Å, allowing H α , [N II] $\lambda\lambda6548,6583$, [S II] $\lambda\lambda6716,6731$, and [O I] $\lambda6300$ to be observed. For the blue lines [O III] $\lambda5007$ and H β , the central wavelength was set to about 5000Å.

For the parallel slit, seven half-hour spectra were taken, along with separate sky exposures because no part of the slit covered pure sky. For the perpendicular slit, seven half-hour spectra were taken covering the blue lines, and three covering the red lines. Sky subtraction for these spectra was achieved using regions of pure sky at both ends of the slit. Exact slit center positions

were varied to allow removal of chip defects in the stacking process.

The reduction was carried out with the IRAF² package. Small-scale variations in response were removed using projector flats. The slit illumination correction was determined with sky flats, and the spectral response function with standard stars. Arc lamp exposures were used to calibrate the wavelength scale as a function of location along the slit. The final calibrated, sky-subtracted spectra were spatially aligned and stacked. The noise in continuum-free regions of the stacked perpendicular slit exposures is 2×10^{-18} and 3×10^{-18} erg cm⁻² s⁻¹ Å⁻¹ arcsec⁻² in the blue and red spectra, respectively. For the stacked parallel slit exposures, continuum covers the entire slit length and consequently the pixel-to-pixel variations are higher: 6×10^{-18} erg cm⁻² s⁻¹ Å⁻¹ arcsec⁻². Since the spectral lines appear well represented by Gaussians, line properties were determined with Gaussian fits. The continuum level was estimated from a linear fit to the continuum on each side of the line. Error bars reflect the noise in the spectra and the uncertainty in the fit of the spectral response function.

Line ratios for the perpendicular slit are consistent with those in R97, given the calibration and slit positioning uncertainties. However, there is a mistake in the velocity scale of Figure 10 of R97: all velocities are about 35 km s⁻¹ too low.

3. Results and Discussion

3.1. The "Parallel" Slit

The H α , [N II], and [S II] lines were detected along the entire useable slit length, which corresponds to about 15 kpc at the assumed distance of NGC 891. Reliable parameters could be measured over a 13 kpc region. [O I] is detected from about 3 kpc SW of the peak in continuum emission to the NE edge of the slit. However, confusion with a sky line limits measurement of reliable parameters on the NE side to a maximum distance of about 5 kpc from the continuum peak. Figure 2 shows the runs of [S II] $\lambda 6716/\text{H}\alpha$, [N II] $\lambda 6583/\text{H}\alpha$, [O I] $\lambda 6300/\text{H}\alpha$, [S II] $\lambda 6716/[\text{N II}]\lambda 6583$, and normalized H α surface brightness with position along the slit. The data have been averaged over 10 pixels, or about 300 pc, except in the case of [O I]/H α , where the averaging is over 20 pixels. Figure 1b shows that the slit traverses four bright filaments. These are apparent as peaks in the H α profile (marked in Figure 2a). The emission is also obviously much brighter on the NE side than on the SW side, confirming the result from the images of RKH and Dettmar (1990). The ratio of the two [S II] lines is consistent with the low-density limit of 1.5 (Osterbrock 1989), even for the filaments.

At first glance, it would seem that the data support the expectation outlined in §I: there is

²IRAF is distributed by the National Optical Astronomy Observatories, which is operated by the Association for Research in Astronomy, Inc., under cooperative agreement with the National Science Foundation.

a definite reduction in [S II]/H α and [N II]/H α at the positions of the four bright filaments. [O I] $\lambda 6300/H\alpha$ also tends to be lower at the filament crossings. However, this result reflects a more general trend of these line ratios with H α surface brightness, as shown in Figure 3. The ratios at the positions of the three brightest filaments define the correlation at H α surface brightnesses ≥ 20 erg cm⁻² s⁻¹ arcsec⁻². There is no evidence for a discontinuity or steepening of the correlation at these intensities. In fact, the slope becomes nearly flat here.

What is the reason for these very good correlations? Very similar results are found for the perpendicular slit data (Figure 7), suggesting, in a stellar photo-ionization scenario, that they reflect the well-established variation (e.g. S94) of line ratios with ionization parameter, U, which measures the diluteness of the radiation field (see §1). If this is the case, then it is implied that U is lower along lines of sight with faint DIG, even when comparing at the same z.

Gas along lines of sight with faint $H\alpha$ emission may be relatively remote from ionizing stars in the disk, so that large columns of intervening gas and geometric dilution result in a low U. Alternatively, it is possible that such gas is no more remote from ionizing stars, but that U is low because the responsible clusters feature fewer such stars, leading to an intrinsically weak emergent ionizing radiation field. The fact that the lines of sight passing through the filaments feature the brightest DIG while the filaments are clearly associated with bright visible HII regions in the disk (Figure 1b) would tend to suggest that the former explanation is correct. However, the dust lane may be hiding numerous fainter HII regions whose stars may be the primary source of ionization for gas along lines of sight with fainter emission. On the other hand, such HII regions should contain fewer massive stars and have, if the IMF varies little, a lower probability of containing the most massive stars, resulting in softer spectra on average. A softer spectrum leads to lower line ratios (S94) and would offset the dilution effect to some degree. This question will probably be resolved from studies of DIG in more face-on galaxies where the in-plane variations of $H\alpha$ surface brightness and line ratios can be related to the distribution of ionizing stars.

Regardless of the explanation, since the filaments in NGC 891 follow the overall correlation in Figure 3, it cannot be claimed that the line ratios are lower in the filaments because they surround *evacuated* regions and are directly ionized by HII regions below. This does not imply that the filaments are not chimney walls, but does point out the potential difficulties in deriving information on isolated structures in edge-on galaxies.

It is interesting that [SII]/[NII] shows almost no spatial variation or dependence on $H\alpha$ surface brightness compared to the other line ratios. This ratio will be discussed further in the next section, where it will become clear that there is little dependence on z either.

Figure 4 shows heliocentric velocity centroids, formed from a weighted average of the $H\alpha$, [S II], and [N II] line centroids, along with the emission profile. One of the filaments on the NE side and a broad region centered on a filament on the SW side show velocities further from the systemic velocity than expected from the smooth, nearly linear trend of velocity with position. Again, this is not necessarily an indication that the filaments have peculiar velocities, but may

simply indicate that they are located in the inner disk. If so, then these velocities are more heavily weighted by inner disk material than are adjacent ones. Inner disk gas will show velocities further from the systemic velocity compared to outer disk gas because of the greater projection of the rotation velocity vector along the line of sight. Hence, the velocity deviations may simply be due to geometrical effects.

3.2. The "Perpendicular" Slit

The H α line, the [N II] $\lambda 6583$ line and the [S II] lines are detected up to about z=3 kpc on each side of the plane. [O I] is detected to about half this height, while [O III] and H β are detected up to about z=2.5 kpc.

Shown in Figure 6 are the vertical runs of [S II] $\lambda 6716/\text{H}\alpha$, [N II] $\lambda 6583/\text{H}\alpha$, [O I]/H α , [S II] $\lambda 6716/[\text{N II}]$ $\lambda 6583$, and [O III]/H β . The H α profile is also plotted – the local minimum at z=0 kpc is due to the dust lane. The data are averaged over 10 pixels. [N II]/H α and [S II]/H α show a smooth and remarkably similar increase with z, from about 0.35 in the midplane to over 1.0 at z=2-3 kpc. [S II]/[N II] is nearly constant at about 0.6 at all z where the uncertainties are not too large. [O I]/H α increases from about 0.03 at z=0 kpc to 0.08 at z=1.3 kpc. However, the most surprising result is that [O III]/H β rises from 0.3 in the midplane to 0.8 at z=2 kpc. Figure 7 shows the correlation of these ratios with H α surface brightness. These are very similar to the correlations in Figure 3. Again, the ratio of the two [S II] lines is everywhere consistent with the low-density limit of 1.5.

Again assuming $T_e = 10^4$ K, [O I]/H α values imply H is essentially 100% ionized at z = 0 kpc, decreasing to about 90% at z = 1 kpc. If $T_e = 8000$ K, then these ionization fractions are 90% and 80%.

Except for the discrepancy mentioned in §2, the mean velocities of the lines are consistent with the results of R97 and give no additional information. Therefore, we will not discuss the kinematics further.

3.2.1. Photo-ionization Models

We now attempt to understand whether the above emission line properties can be understood by massive-star photo-ionization alone. In doing so, we temporarily ignore the problems posed by the low $\text{He\,I/H}\alpha$ but will return briefly to the reconciliation of this ratio with the forbidden line ratios in §4. We use unpublished models from S94 since they are the only models which specifically attempt to reproduce the line ratios in the DIG of NGC 891. In these models an ionizing spectrum of radiation from a population of stars with an IMF slope of -2.7 (intermediate between Salpeter and Miller-Scalo values) and stellar atmospheres from Kurucz (1979) is considered. This

radiation field is allowed to propagate through a slab of gas (representing a clump of halo gas) in a one-dimensional calculation, the dilution being measured by the ionization parameter, U, at the front of the slab. As discussed in §1, as lower values of U are considered, the predominant ionization state of S and O (and N to a lesser extent) changes from doubly to singly ionized. As a consequence, [N II]/H α and [S II]/H α rise while [O III]/H β falls. At the end of the model slab, an increasingly neutral zone appears as lower values of U are considered, leading to a slow rise in [O I]/H α with U. In this one-dimensional calculation of pure photo-ionization, U is expected to decline exponentially with z. This dependence is probably more complicated in a real galaxy, although U should generally fall with increasing height. Thus, further free parameters are the value of U at z = 0 kpc, and the run of U with z.

Both radiation bounded models and matter bounded models with various terminating total atomic hydrogen columns for the clumps were considered by S94. We will use only his models with the hardest stellar spectrum considered (with an upper IMF cutoff of 120 $\rm M_{\odot}$), hardening of the radiation field as it propagates through the intervening gas before reaching the slab, and heavy element depletions. Only these models are able to yield [N II]/H α and [S II]/H α in the range 1–1.5. These models have also been recently published by Bland-Hawthorn et al. (1997). We examine as two extremes the matter-bounded model (which will be referred to as PM) with the lowest terminal hydrogen column considered for the individual clumps, 2×10^{18} cm⁻², and the radiation-bounded model (PR).

Figures 8 and 9 show these ratios in diagnostic diagrams of $[O\,III]/H\beta$ and $[O\,I]/H\alpha$ vs. $[N\,II]/H\alpha$ and $[S\,II]/H\alpha$, and $[S\,II]/H\alpha$ vs. $[N\,II]/H\alpha$. Along the sequence of points, z generally increases from 0 kpc at the left end to 2 kpc for plots of $[O\,III]/H\beta$, 1.3 kpc for $[O\,I]/H\alpha$, and 3 kpc for $[S\,II]/H\alpha$ vs. $[N\,II]/H\alpha$ at the right end. Models PR and PM are shown in Figures 8 and 9 as the small open circles joined by solid lines. Values of $\log U$ are marked as explained in the captions.

It is immediately obvious that neither model is a good match to the data. Most importantly, the flatness of $[O\,III]/H\beta$ below z=1 kpc and its rise with $[N\,II]/H\alpha$, $[S\,II]/H\alpha$ (and z) above z=1 kpc is at complete odds with the models. Also, the typical value of $[O\,III]/H\beta$ is poorly predicted by a model chosen to match the observed $[N\,II]/H\alpha$ and $[S\,II]/H\alpha$. In model PR, while $[N\,II]/H\alpha$ and $[S\,II]/H\alpha$ require $\log U$ in the range -2.3 to -2.7 at z=0 kpc, and -3.3 to -3.7 at z=2 kpc, the predicted $[O\,III]/H\beta$ is $\gtrsim 10$ times that observed for most of this range of U.

In model PM, on the other hand, if we use [N II]/H α and [S II]/H α to set U at z=0 kpc, we require $\log U$ in the range -3.7 to -4.1, and an extra source of [O III] emission at lower U. While such a source can be identified and tested (see below), it is not clear that such a low value of U should apply to the midplane, given that the disk contains both HII regions and diffuse gas. However, at low z the kinematics indicate that we receive emission preferentially from the outer disk because of the absorbing dust layer (R97). This outer disk gas may, like the high-z gas, see a relatively dilute radiation field because star formation is concentrated in the inner disk (Rand

1997b). In that case the appropriate U for z = 0 may be quite low and the gradient of U with z rather shallower than expected in a galaxy without such a dust lane.

Both models are more successful at reproducing the runs of [O I]/H α vs. [N II]/H α , [O I]/H α vs. [S II]/H α and [S II]/[N II]. If [N II]/H α were lower by about -0.2 dex at low z, PR would fit these data quite well, with $\log U = -2.6$ at z = 0 kpc, -3.3 at z = 1 kpc, and -3.7 at z = 2 kpc. Model PM would fit equally well for $\log U = -4.0$ at z = 0, -4.5 at z = 1 kpc, and -5.0 at z = 2 kpc. A similar discrepancy in the observed vs. modeled vertical run of [S II]/[N II] was noted by Golla et al. (1996) in NGC 4631. [N II]/H α is expected to show less disk-halo contrast than [S II]/H α because the change in predominant ionization state between HII regions and diffuse gas is smaller for N due to its higher ionization potential. This trend is reflected in the models of both S94 and Domgörgen, & Mathis (1994). In both NGC 891 and NGC 4631, however, the disk-halo contrast in [S II]/H α is rather similar to that in [N II]/H α .

One important factor in explaining the common behavior of [SII]/H α and [NII]/H α might be a radial abundance gradient in league with the dust absorption effect noted above. Rubin, Ford, & Whitmore (1984) found that log ([SII]/[NII]) generally increases in HII regions in spirals by 0.3 "from inner to outer HII regions". If such a gradient is present in NGC 891, then the fact that we preferentially observe outer disk gas at low-z means that [SII]/[NII] should be higher there for a given U. The gradual inclusion of more inner disk gas with increasing z will then tend to offset the dependence of [SII]/[NII] on U in the models. However, the parallel slit data suggests little dependence of the ratio on distance along the major axis, although there is a slight trend in the right direction between 2 and 7 kpc from the center on both sides. Hence, inasmuch as the major-axis dependence of [S II]/[N II] at z = 700 pc reflects the radial dependence at z = 0pc, it would seem that an abundance gradient does not affect the line ratios significantly. Other expected effects of an abundance gradient are also not seen in the parallel slit data. Domgörgen, & Mathis (1994) find that [N II]/H α and [S II]/H α increase with abundance, while [O I]/H α shows little dependence. In the presence of a radial gradient, these trends, if strong enough, might be revealed as a decline in $[NII]/H\alpha$ and $[SII]/H\alpha$ with distance along the major axis. The dominant trend there is with $H\alpha$ brightness and thus it seems that variations in U are the more important effect. Again, though, it must be noted that the averaging along the line of sight in the parallel slit data will diminish the observable effects of an abundance gradient. So far, it has been difficult to find much variation in [SII]/[NII] in the DIG of edge-on galaxies. This question remains open to further exploration.

3.2.2. Composite Photo-ionization and Shock Models

The most surprising result for the perpendicular slit is the behavior of $[O\,III]/H\beta$ with z. Although such high (and higher) values of $[O\,III]/H\beta$ are found in HII regions, they are a feature of high-excitation (high U) conditions. If the level of excitation were increasing with z, however, we would also expect to see $[N\,II]/H\alpha$ and $[S\,II]/H\alpha$ falling, contrary to what is observed. As

discussed above, their rise is qualitatively consistent with a smooth transition from predominantly doubly-ionized to singly-ionized states, as expected in the dilute photo-ionization models. Hence, it is very unlikely that the [O III] emission arises from the same DIG component as the [N II] and [S II]. We therefore require a second source of diffuse $H\alpha$ emission which features bright [0 III]. Two plausible mechanisms for producing such emission, shocks and turbulent mixing layers are discussed in this and the next subsection. respectively. Both can produce bright [O III] emission. These mechanisms were also considered for DIG in irregular galaxies by M97. It should be noted, though, that the DIG in these irregulars is generally much brighter than that studied here.

We first consider whether the line ratio data can be explained if some of the DIG emission is produced by shock ionization. We consider only the PM model further because the PR model would require a second source of $H\alpha$ emission with highly unusual properties: if the value of U at the midplane is to be roughly -2.3 to -2.7, then the second component must dominate the stellar-ionized component by a factor of 30 or more and have essentially no [O III] emission if the runs of [O III]/H β vs. [S II]/H α and [N II]/H α are to be explained. Low-speed shocks do have this property, but also produce large amounts of [O I] emission, further confouding the problem. Alternatively, if $\log U \sim -4.0$ at z=0 kpc, then the second component must have essentially no [N II] or [S II] emission and account for about 75% of the H α emission at z=0 kpc in order to reproduce the values of [S II]/H α and [N II]/H α . In either case, it is also difficult to see how the subsequent rise in all the line ratios with z would be achieved without the model being highly contrived. With the PM model, there is some hope of matching the data by adding a strong source of [O III] emission as long as U is low enough in the midplane and the other ratios can be matched.

We employ the shock models of Shull & McKee (1979), as were also considered by M97. The line ratios in shock models, especially [O III]/H β , are very sensitive to the shock velocity. Other variables include the preshock gas density and ionization state, abundance, and transverse magnetic field strength. The gas is assumed to be initially neutral at $n_0 = 10$ cm⁻³ and subsequently penetrated by a precursor ionization front. More appropriate to our case would be a lower initial density (of order 0.1 cm⁻³) and a high initial ionization fraction. We should also consider depleted abundances to be consistent with the stellar ionization models, but SM calculated only one such model to show the general effect of depletions. We do not perform an exhaustive search of parameter space or carry out a statistical test of the goodness of fit, firstly because an examination of figures such as Figure 9 can quickly reveal which composite models are most successful, and secondly because some of the fixed parameters are probably inappropriate for the halo of NGC 891 in any case.

In the composite models, we still consider that the stellar radiation field is characterized by a decrease of U with z, and that some fraction of $H\alpha$ emission from shock ionization is added, with this fraction possibly changing with z. Although no model can reproduce the line ratio behavior to within the errors, we find that some of the main characteristics of the data can be reproduced. One of the most successful models is shown overlaid on the data in Figure 9 as the dashed lines joining open circles, which mark values of $\log U$. The shock speed is 90 km s⁻¹. At z = 0 kpc, 7%

of the H α emission arises from a 90 km s⁻¹ shock, rising to 30% by z=2 kpc. The composite model is most successful if $\log U=-4.0$ at z=0 kpc, -4.5 at z=1 kpc (the limit of the [O I]/H α data), and -5.0 at z=2 kpc (the limit of the [O III]/H β data). Note that in the figure, circles indicate $\log U=-4.0$, -4.3, -4.7 and -5.0, corresponding to z=0-2 kpc, in all the panels despite the fact that the [S II]/[N II] ratio includes data up to z=3 kpc and [O I]/H α is only detected up to z=1 kpc. Also shown in Figure 9 are the line ratios for the shock models alone, namely, a 90 km s⁻¹ and a 100 km s⁻¹ shock with standard abundances, and a 100 km s⁻¹ shock with depleted abundances.

The major shortcoming of this composite model is in reproducing [S II]/[N II] at low z. For a given amount of [S II] emission, the model overpredicts [N II]. At high z this ratio is somewhat more successfully modeled, but [N II]/H α simply does not show as much disk-halo contrast as observed, as was the case for the pure photo-ionization models. Also, the predicted [S II]/H α and [N II]/H α reach a plateau at 1.0 at the lowest U considered by S94, and thus cannot match the observed continuing rise beyond z=2 kpc (Figure 9e). In this regard radiation-bounded models are more successful (S94), at least for [S II]/H α . In that model, it is still rising at the lowest considered U value, so that its observed continued rise may be explainable. Finally, a low value of U at z=0 pc is still required, but again this may not be unreasonable given the arguments mentioned above.

There is some freedom for variation of the shock parameters. A 130 km s⁻¹ shock (the highest speed considered by SM) contributing 2% of the H α emission at z=0 kpc, rising to 7% at z=2 kpc, produces almost identical curves in the diagnostic diagrams. Since only the [O III]/H β ratio is large (7.35) for this model, adding such a small amount of this emission affects mainly this ratio. The composite model can be further explored by keeping the shock contribution constant with z but varying the shock speed. A model with a shock giving rise to 25% of the H α emission, with a speed of 60 km s⁻¹ at z=0 kpc, and 90 km s⁻¹ at z=2 kpc (but with $\log U=-4.7$ now) can reproduce the ranges of [S II]/H α , [N II]/H α , [S II]/[N II], and [O III]/H β as successfully as the above models, but low-speed shocks produce far too much [O I] emission.

SM find that the effect of introducing depleted abundances for a 100 km s⁻¹ shock is to raise [S II]/[N II], while [O III]/H β drops and [O I]/H α rises. However, assuming that the fractional changes also apply for a 90 km s⁻¹ shock, depleted abundances do not solve the [S II]/[N II] problem, even if the composite model is started at a different value of log U. The effect on [S II]/[N II] is insufficient because of the small contribution from shocks needed to fit [O III]/H β .

Further latitude in the composite models may be gained by considering a larger range of values for some of the other variables. For instance, Dopita & Sutherland (1996) calculate properties of lower density, magnetized shocks with speeds from 150 to 300 km s⁻¹. They consider densities and magnetic field strengths obeying the relation $0 < B/n_e^{1/2}(\mu \text{G cm}^{3/2}) < 4$. These shocks have strong radiative precursors which contribute a significant fraction of the emission. A model with shock speed 150 km s⁻¹, $n_e = 1 \text{ cm}^{-3}$ and no magnetic field produces line ratios similar to the 90

km s⁻¹ model considered above, with the exception that $[O\ I]/H\alpha$ is about 80% higher. The main conclusion from this subsection is that shocks are feasible as a secondary source of energy input into the DIG of NGC 891, but it is difficult to constrain their parameters with much confidence.

We have not speculated on the origin of the putative shocks. But given that the observed filaments suggest the presence of supershells and chimneys, it is plausible that the shocks originate in such expanding structures. The shock speeds considered above are reasonable when compared to superbubble calculations (e.g. MacLow, McCray, & Norman 1989). In fact, the slit passes close to one of the most prominent filaments, which may still have an associated shock. This possibility highlights the importance of observing with many such slit positions.

Finally, we point out that M97 also found that if a constant shock speed model is used, then the fraction of the DIG emission that must come from shocks increases with z.

3.2.3. Composite Photo-ionization and Turbulent Mixing Layer Models

Turbulent mixing layers (TMLs) are expected to occur at the interfaces of hot and cold (or hot and warm) gas in the ISM of galaxies (Begelman & Fabian 1990; Slavin, Shull, & Begelman 1993). Superbubble walls are a likely location for such layers. Shear flows are expected along the interface, leading to Kelvin-Helmholtz instabilities and subsequent mixing of the gas. The result is a layer of "intermediate temperature" gas, probably at $5.0 \leq \log T \leq 5.5$. This gas may produce some fraction of the DIG emission in galaxies. Like typical DIG, it features enhanced [S II]/H α and [N II]/H α relative to HII regions and low [O I]/H α . However, unlike stellar-ionized gas, [O III]/H β should be of order 1–3. Hence, TMLs provide a source of enhanced [O III]/H β and therefore may be relevant to the current problem.

Slavin, Shull, & Begelman (1993) calculate line ratios for TMLs as a function of shear velocity, mixing layer temperature, initial cold layer temperature, and abundance (solar vs. depleted). We will consider depleted abundances here. Again, we will introduce a contribution to the DIG emission from TMLs at some z or U, allowing for an increase in this contribution with z as U continues to decline, and consider only the PM model for the photo-ionized component. The best match to the data features a shear velocity of 25 km s⁻¹ (the lowest modeled), a mixing layer temperature of $\log T = 5.3$, and an initially warm layer at 10^4 K rather than a cold layer. This model is shown overlaid on the diagnostic diagrams in Figure 10. At z = 0 kpc, 3% of the H α emission arises from TMLs, rising to 15% at z = 2 kpc. The rough relation of $\log U$ with z is similar to the previous composite model: $\log U = -4.1$ at z = 0 kpc, -4.5 at z = 1 kpc (the limit of the $[O II]/H\alpha$ data), and -5.0 at z = 2 kpc (the limit of the $[O III]/H\beta$ data). Again, note that in the figure, circles indicate $\log U = -4.1$, -4.3, -4.7 and -5.0, corresponding to z = 0 - 2 kpc, in all the panels despite the varying maximum z of the line ratio determinations.

The model is reminiscent of the best shock models and appears to be somewhat more successful, but suffers from the same primary shortcoming: the underprediction of [S II]/[N II]

at low z. Other TML models will not alleviate this problem because the model in Figure 10 already features maximal [S II]/[N II]. As is the case for shocks, there is room for flexibility in the parameters. For instance, [O III]/H β is fairly constant in all the models with depleted abundances, and all models regardless of abundance feature very low [O I]/H α . [S II]/H α and [N II]/H α show somewhat more variation with the input parameters, but as most of the [S II] and [N II] emission arises from the stellar-ionized gas, and the TML contribution is small, there is reasonable latitude for variation of the parameters without altering the resulting values of these ratios. Again, the main point is to demonstrate the feasibility of TMLs as a secondary source of energy input rather than to find the best fitting parameters, or indeed to show whether TMLs or shocks are preferred as the second component.

3.2.4. Other Possible Sources of Energy Input

Shapiro & Benjamin (1993) consider cooling, falling galactic fountain gas initially raised from the midplane by supernovae. The calculation is followed from an initial temperature of 10^6 K to a final value of 10^4 K. While there are not yet predictions of optical emission line ratios from such gas, one can expect [O III] emission as the gas cools. The run of [O III]/H β with z in a composite model with fountain gas would depend on the fraction of diffuse H α emission produced by the latter (the authors estimate that it could account for perhaps 40% in the Milky Way) and the details of the cooling and dynamics, including the interaction with halo gas from other processes.

Another idea that has not been deeply explored is heating of the halo by microflares from magnetic reconnection events (Raymond 1992). This process may have a role in producing ultraviolet emission and absorption lines, soft X-ray halo emission, and Reynolds layer emission. As the theory stands now, a broad range of $[O\,III]/H\alpha$ values may result from this process, and there are enough uncertainties as not to warrant a detailed comparison with the data at this point. The relevance of microflares should be revealed with further refinements of the theory and additional observations.

The problem of explaining low $\text{He\,I/H}\alpha$ in combination with high [S II]/H α and [N II]/H α has motivated work on other sources of heating for the DIG. Since the forbidden lines are highly temperature sensitive, small changes in temperature can be important. Minter & Balser (1997) find that the dissipation of turbulent energy in the ISM could raise the temperature of the DIG by about 2000 K without additional ionization of helium, thus providing a reasonable match to these line ratios in the Reynolds layer. However, there is still insignificant [O III] emission. Photo-electric heating from dust grains (Reynolds & Cox 1992) should also have little effect on [O III] emission.

Finally, scattered light from HII regions could be a source of [O III] emission in the halo, but the rise in $[O III]/H\beta$ with z would not be expected.

4. Discussion and Conclusions

Using a slit oriented parallel to, and offset 700 pc above, the major axis of NGC 891, a spectrum of the DIG has been taken which reveals a clear correlation of ratios of forbidden lines to $H\alpha$ with the $H\alpha$ surface brightness. The original motivation for this observation was to search for variations in line ratios on and off the filaments of DIG as further evidence that they are walls around evacuated chimneys. But although the filaments do show reduced $[SII]/H\alpha$, $[NII]/H\alpha$, and $[OI]/H\alpha$ relative to gas on adjacent lines of sight, the contrast merely reflects the overall correlation. The relationship probably indicates that regions of brighter $H\alpha$ emission receive a radiation field with a higher ionization parameter. Also, although some of the filaments show deviations from the observed smooth trend of mean velocity with position along the major axis, these departures could simply be due to geometric effects: if the filaments are inner galaxy features, they will bias the mean velocity for their line of sight away from the systemic velocity. [SII]/[NII] surprisingly shows no significant variation along the slit. Finally, the $H\alpha$ -emitting halo gas at this height is about 80–95% ionized, based on the observed range of $[OI]/H\alpha$ and assuming $T = 10^4$ K. The correlation of $[OI]/H\alpha$ with surface brightness probably reflects a higher degree of ionization where the photon field is more intense.

Results from this observation emphasize the difficulty in interpreting DIG observations of edge-on galaxies. Confusion is caused by uncertainties in the location of a parcel of gas along the line of sight, its effective distance from a source of ionization and other unrelated gas in the same direction. It is difficult from such observations to draw conclusions about the environment of the filament, for example.

Spectra from a slit oriented perpendicular to the plane at R=100'' along the major axis on the NE side show a rise of [S II]/H α , [N II]/H α , and [O I]/H α with z. At the midplane, [O I]/H α values indicate that H is essentially 100% ionized, dropping to 90% at z=1 kpc, assuming $T=10^4$ K. The z-dependence of these line ratios is expected if the gas is ionized by massive stars in the disk. However, it is unexpectedly found that [O III]/H β also rises with z, whereas it should decline with z in photo-ionization models. This result necessitates the consideration of secondary sources of ionization. [S II]/[N II] unexpectedly shows essentially no dependence on z and H α surface brightness. Put another way, [N II]/H α shows the same disk-halo contrast as that of [S II]/H α , whereas a smaller contrast is expected.

Strong [O III] emission is expected from several energetic processes. We considered shocks and turbulent mixing layers as sources of such gas. Models in which a small fraction of the ${\rm H}\alpha$ emission comes from one of these mechanisms can be made to fit the data reasonably well, but most noticeably the remarkable constancy of [S II]/[N II] with z is still difficult to reproduce. In the case of shocks, it is difficult to constrain the shock speed or the contributed fraction of the DIG emission at this point. Of course, the line of sight may sample shocks with a range of speeds and some mean value. There is also significant latitude in the parameters in the case of TMLs. Other sources of strong [O III] emission may include cooling galactic fountain gas and microflares

from magnetic reconnection. These should be explored further in light of the current results. Because of these facts and possibilities, the results are meant only to indicate the feasibility of such classes of models and the likelihood that one or more physical processes is producing intermediate temperature gas in the halo of NGC 891.

On the other hand, the finding that the second source of line emission becomes more important as z increases may be reasonable. In the case of TMLs, for example, Shull & Slavin (1994) point out that this process may indeed be more common at large z, where superbubbles break out of the thin disk gas layers, producing Rayleigh-Taylor instabilities and shear flows that lead to the mixing. These authors were attempting to explain the larger scale-height of CIV UV absorption line gas relative to NV (Sembach & Savage 1992) as an increasing predominance of TMLs over SN bubbles with height off the plane – the former producing higher CIV/NV. If the TML process begins only at the approximate height where breakout occurs, while the stellar radiation field is increasingly diluted with z, then an increasing fraction of H α emission from TMLs may be quite reasonable. The rough fractions found in §3.2.3 are comparable to those expected by Slavin et al. (1993) for the Milky Way diffuse H α emission.

If the photo-ionized and secondary components of the DIG emission both arise in exponential layers with different scale-heights, then the composite models, although illustrative, can be used to estimate roughly the relative scale-heights. In the two shock models and one TML model considered, the fraction of emission arising from the second component is 3–5 times higher at z=2 kpc than at z=0 kpc. Assuming exponential layers, the scale-height of the second component must be 3–4 times that of the photo-ionized component. This conclusion is very tentative, however, given the uncertainties in the modeling and the lack of information on $[O\ III]/H\beta$ at higher z. It it is tempting to identify the second component with the high-z tail of $H\alpha$ emission found in the deeper spectrum of Rand (1997a). However, the exponential scale-height of this tail is 5–7 times that of the main component, and it contributes about 50% of the emission at z=2 kpc. While these numbers do not quite match those for the second component proposed here, there may yet prove to be a connection.

For the photo-ionized component, we found the most success by using the model from S94 with the lowest terminal hydrogen column considered for individual clouds in the DIG layer. Using larger columns tends to push the model curves towards those of the radiation-bounded case, which is found to be very difficult to incorporate in a successful composite model. This constraint suggests that the DIG consists of quite small clumps (or filaments or sheets, since S94's calculation is one-dimensional) of several pc thickness, for a representative density of $n_e = 0.1 \text{ cm}^{-3}$. If this conclusion is not borne out by future observations, the composite models presented here will need to be reconsidered. The S94 model used here also features the hardest emergent stellar spectrum considered (in order to produce high [S II]/H α and [N II]/H α), but more modest spectra may be allowable if other sources of non-ionization heating are at work (e.g. Minter & Balser 1997).

Despite complications introduced by the second DIG component, it should be noted that

the observed properties of the three ratios [S II]/H α , [N II]/H α , and [O I]/H α with z are still reasonably explained to first order by photo-ionization models alone. Their smooth increase with z is as predicted as are their rough values. Emission from the second component probably has only a secondary effect on these ratios. The z-independence of [S II]/[N II] is not understood in either a pure photo-ionization or composite model.

An undesirable aspect of the composite models considered here is that emission from photoionized and (for example) shock ionized gas is simply added together with no unified physical picture in mind. It would be desirable eventually to have, say, a calculation of the evolution of a superbubble which included photo-ionization, shocks and TMLs in a more self-consistent way. For instance, what is the effect of the radiative precursor of a shock which enters gas already ionized by dilute stellar radiation?

The emission line properties revealed by the perpendicular slit share some similarities with those of the halo of the starburst galaxy M82. In the Fabry-Perot data of Shopbell & Bland-Hawthorn (1997), [N II]/H α shows a general tendency to rise with z on the N side, up to the limit of measurability at about z=750 pc. On the S side, there is little dependence on z, with perhaps 0.6 typical. [O III]/H α =0.03 at z = 0 pc and 0.08 at z = 750 pc (values of [O III]/H β are about 3 times higher assuming little extinction). In a long-slit spectrum through the halo of M82, M97 sees higher values of [O III]/H β , reaching 0.7 at z = 1 kpc. The sequence of points in her diagnostic diagram of [S II]/H α vs. [O III]/H β has a rising slope, as in NGC 891, although much steeper (other irregulars show a falling or nearly flat slope). [O I]/H α also rises with z in M82, and shows a range of values (about 0.01 to 0.1) similar to those reported here. Shopbell & Bland-Hawthorn (1997) point out that their ratios become more shock-like with distance from the starburst, as also noted by Heckman, Armus, & Miley (1990). This behavior is now seen in a spiral halo as well.

Other evidence for multi-phase halos is provided by the study of NGC 4631 by Martin & Kern (1998). They detect an extensive halo of [O III] emission which spatially coexists with the observed soft X-ray and H α emitting halos. Within this halo are several bright [O III] condensations in which the measured [O III]/H β ratio is ~ 20 . On this basis, they argue that the H α and [O III] emission is tracing distinct components in a multi-phase halo medium.

It should be pointed out that $[O\,III]/H\alpha$ values of 0.12–0.21 (comparable to values in NGC 891) are seen in the DIG of M31 (Greenawalt et al. 1997). There is little correlation of this ratio with the brightness of the DIG or its remoteness from visible HII regions. The high $[O\,III]/H\alpha$ in this case may be due to a radiation field not as dilute as in the halo of NGC 891 (for instance, $[N\,II]/H\alpha$ and $[S\,II]/H\alpha$ are substantially lower than in the halo of NGC 891 at z=1-2 kpc). Greenawalt et al. (1997) also find that TMLs may contribute some fraction of the $H\alpha$ emission in regions of very faint DIG, but no more than about 20% and most likely only a few percent, similar to the findings for NGC 891.

More light has been shed on the question of $[OIII]/H\beta$ trends in the DIG of face-ons by

Wang et al. (1997). For three of their five galaxies with good [O III] detections in their DIG spectra, they find that $[O III]/H\beta$ is in the range < 0.2 to 2 and, for a given slit, is systematically higher than in the HII regions in that slit. They also find that the [O III] line widths are usually larger than those of [N II], and thus refer to a "quiescent" photo-ionized DIG component which accounts for the bulk of the $H\alpha$, [N II] and [S II] emission, and a "disturbed" component (shocks and TMLs are considered) contributing a minority (< 20%) of the $H\alpha$ emission but responsible for the [O III] emission. For vertical hydrostatic equilibrium, the contrast in line-widths indicates that the scale-height of the disturbed component is 1.5–2 times greater than that of the quiescent DIG. In NGC 891, the line-widths are dominated by galactic rotation and thus such an analysis cannot be carried out.

The existence of a second source of line emission may be relevant for the issue of the low $\text{He I/H}\alpha$ ratio. The value of 0.027 for the lower halo of NGC 891 implies a much softer spectrum than is required to explain the high $[NII]/H\alpha$ and $[SII]/H\alpha$ (R97). Apart from the possibility that the forbidden line emission is complicated by additional sources of ionization and non-ionizing heating, He I/H α may also be affected by secondary ionization sources if they contribute sufficient $H\alpha$ emission. For instance, the ratio is fairly sensitive to shock conditions. The SM 100 km s⁻¹ model gives a value of 0.027. The ratio is 0.005 for an 80 km s⁻¹ shock, but this model predicts insignificant [O III] emission. The Dopita & Sutherland (1996) higher velocity, lower density (n=1), magnetized models give a much more significant ionized precursor. For the lowest velocity considered, 150 km s⁻¹, the shock itself gives a low ratio of 0.019, but the line fluxes for the precursor are not given. For a 200 km s⁻¹ shock, the ratio from combined shock and precursor is 0.046. Slavin, Shull, & Begelman (1993) do not predict He I emission. Regardless, if shocks or TMLs can provide, say 25% of the H α emission at z=2 kpc, then there may be a region of parameter space which can produce low enough He $I/H\alpha$ so that the composite line ratio is significantly reduced below that of the stellar-ionized gas alone. The contributions of these sources required in §3 may not be sufficiently large, but the effect is worth future consideration. The inferred stellar temperature, mean spectral type and upper IMF cutoff would then all be underestimated.

Finally, it is worth re-emphasizing that all emission line fluxes and ratios presented here are averaged along a line of sight through the DIG layer, and that local variations in, for example, the derived ionization fraction of H surely exist. Also, although the vertical dependence of the line ratios has been very revealing, only one slit position has been observed, covering the halo above the most active region of star formation in the disk, and close to an H α filament. A key question is how these halo properties vary with environment. Does [O III]/H β show the same behavior above more quiescent parts of the disk? Is this behavior peculiar to the halo of NGC 891 only, or is it a general feature of DIG halos? These questions will be addressed by further observations.

Reynolds, R. Walterbos (whose comments as referee also improved the paper), J. Slavin, R. Benjamin, J. Shields, and others. The help of the KPNO staff is also greatly appreciated.

REFERENCES

Baldwin, J. A., Phillips, M. M., & Terlevich, R. 1981, PASP, 93, 5

Begelman, M. C., & Fabian, A. C. 1990, MNRAS, 244, 26P

Bland-Hawthorn, J., Freeman, K. C., & Quinn, P. J. 1997, ApJ, 490, 143

Dettmar, R.-J. 1990, A&A, 232, L15

Dettmar, R.-J. 1992, Fund. Cosmic Phys., 15, 143.

Dettmar, R.-J., & Schulz, H. 1992, A&A, 254, L25.

Domgörgen, H., & Mathis, J. S. 1994, ApJ, 428, 647

Dopita, M. A., & Sutherland, R. S. 1996, ApJS, 102, 161

Golla, G.; Dettmar, R. -J., & Domgörgen, H. 1994, A&A, 313, 439

Greenawalt, B., Walterbos, R. A. M., & Braun, R. 1997, ApJ, 483, 666

Haffner, M., & Reynolds, R. J. 1997, preprint

Heckman, T. M., Armus, L., & Miley, G. K. 1990, ApJS74, 833

Heiles, C., Koo, B.-C., Levenson, N. A., & Reach, W. T., 1996, ApJ, 462, 326

Hunter, D. A., & Gallagher, J. S. 1990, ApJ, 362, 480

Kurucz, R. L. 1979, ApJS, 40, 1

MacLow, M.-M., McCray, R., & Norman, M. 1989, ApJ, 337, 141

Martin, C., & Bowyer, S. 1990, ApJ, 350, 242

Martin, C., & Kern 1998, submitted to ApJ

Martin, C. L 1997, ApJ, 491, 561

Mathis, J. S. 1986, ApJ, 291, 247

Minter, A. H., & Balser, D. S. 1997, preprint

Norman, C. A., 1991 in IAU Symp. 144, The Interstellar Disk-Halo Connection in Galaxies, (Dordrecht: Kluwer), ed. H. Bloemen, 337

Norman, C. A., & Ikeuchi, S. 1989, ApJ, 345, 372

Osterbrock, D. E. 1989, Astrophysics of Gaseous Nebulae and Active Galactic Nuclei (Mill Valley: University Science Books)

Rand, R. J. 1996, ApJ, 462, 712

Rand, R. J. 1997a, ApJ, 474, 129 (R97)

Rand, R. J. 1997b, in Gas Disks in Galaxies, ed. J. M. van der Hulst (Kluwer), 105

Rand, R. J., Kulkarni, S. R., & Hester, J. J. 1990, ApJ, 352, L1 (RKH)

Raymond, J. C. 1992, ApJ, 384, 502

Reynolds, R. J. 1984, ApJ, 282, 191

Reynolds, R. J. 1985, ApJ, 294, 256

Reynolds, R. J. 1989, ApJ, 345, 811

Reynolds, R. J. 1992, ApJ, 392, L35

Reynolds, R. J. 1993, in Back to the Galaxy, ed. S. S. Holt & F. Verter (A.I.P. Conf. Proc. 278), 156

Reynolds, R. J., & Cox, D. P. 1992, ApJ, 400, 33

Reynolds, R. J., & Tufte, S. L. 1995, ApJ, 439, L17

Rubin, V. C., Ford, W. K. Jr., & Whitmore, B. C. 1984, ApJ, 281, 21

Sembach, K. R., & Savage, B. D. 1992, ApJS, 83, 147

Shapiro, P. R., & Benjamin, R. A. 1993, in Star Formation, Galaxies, and the Interstellar Medium, eds. J. Franco, F. Ferrini, & G. Tenorio-Tagle (Cambridge Univ. Press), 275

Shopbell, P. L., & Bland-Hawthorn, J. 1997, ApJ, in press

Shull, J. M., & McKee, C. F. 1979, ApJ, 227, 131 (SM)

Shull, J. M., & Slavin, J. D. 1994, ApJ, 427, 784

Slavin, J. D. Shull, J. M. & Begelman, M. C. 1993, ApJ, 407, 83

Sokolowski 1994, preprint (S94)

Swaters, R. 1994, Doctoraal Scriptie, Univ. Groningen

Veilleux, S., & Osterbrock, D. E. 1987, ApJS, 63, 295

Walterbos, R. A. M. 1997, preprint

Walterbos, R. A. M. & Braun, R. 1994, ApJ, 431, 156

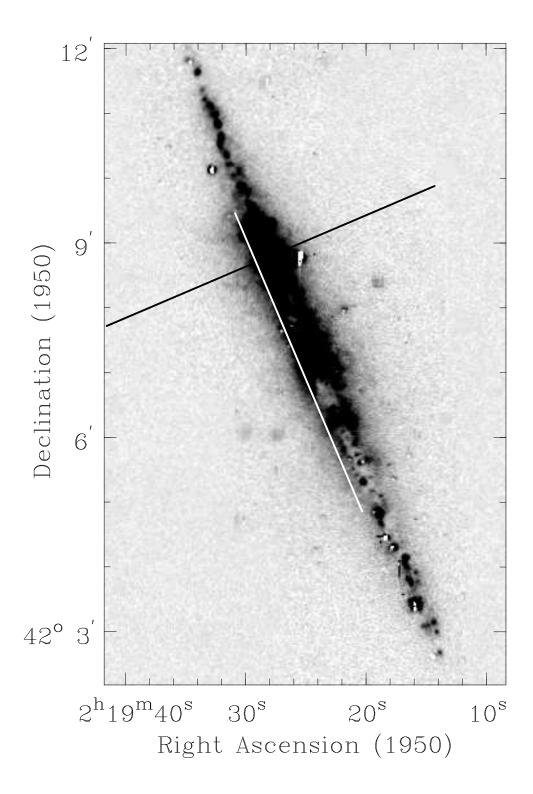
Wang, J., Heckman, T. M., & Lehnert, M. D. 1997, preprint

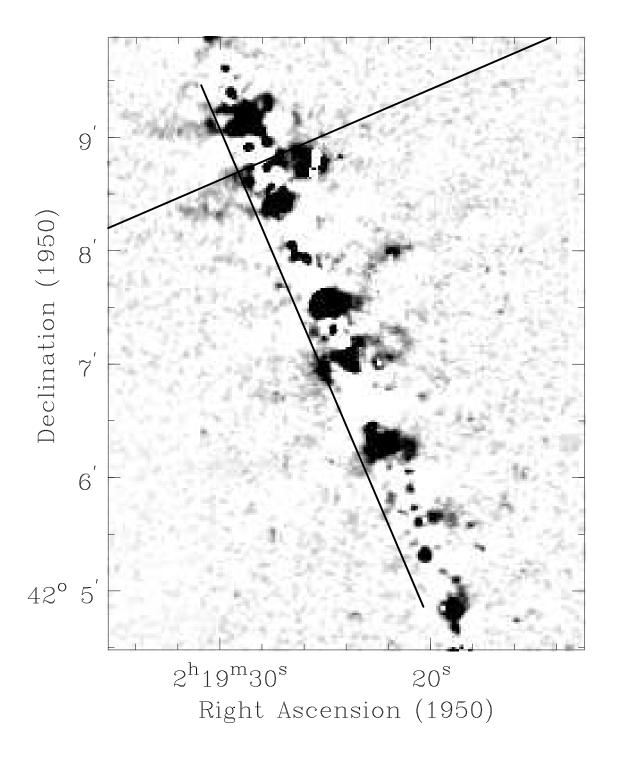
This preprint was prepared with the AAS IATEX macros v4.0.

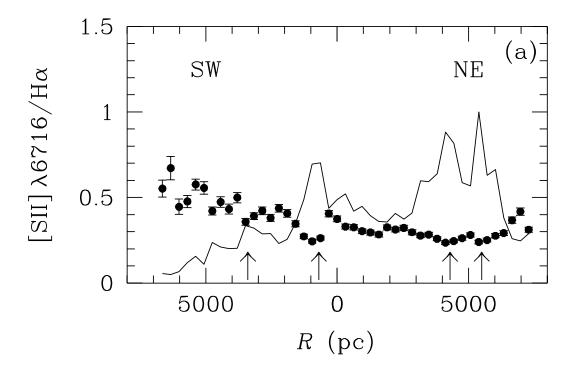
- Fig. 1.— The slit positions for the two observations are shown overlaid on the H α image of NGC 891 from Rand, Kulkarni, & Hester (1990) in (a), and on a version of the central part of the same image in (b), processed to show how the "parallel" slit traverses filaments of H α emission (see text).
- Fig. 2.— Dependence of line ratios on slit position for the parallel slit. In each panel, the normalized H α surface brightness is plotted. Positions of the four brightest filaments are indicated with arrows in (a). The line ratios plotted are (a) [S II] λ 6716/H α , (b) [N II] λ 6583/H α , (c) [O I] λ 6300/H α , and (d) [S II] λ 6716/[N II] λ 6583.
- Fig. 3.— The dependence of (a) [N II] $\lambda 6583/\text{H}\alpha$ (filled symbols), [S II] $\lambda 6716/\text{H}\alpha$ (open symbols), and (b) $3\times[\text{O I}]$ $\lambda 6300/\text{H}\alpha$ (filled symbols) and [S II] $\lambda 6716/\text{H}\alpha/[\text{N II}]$ $\lambda 6583/\text{H}\alpha$ (open symbols) on $\text{H}\alpha$ surface brightness. Triangles indicate data points at locations of filaments marked in Figure 2. Note that the [O I]/ $\text{H}\alpha$ values and error bars have been multiplied by 3.
- Fig. 4.— The intensity-weighted mean heliocentric velocity vs. location determined from the H α , [S II], and [N II] lines. Note some deviations from the general trend at the positions of filaments, which are indicated by arrows. Velocity uncertainties generally increase with decreasing intensity and are 1-2 km s⁻¹ for all points except those to the SW of the lowest intensity filament, where they rise to 3-5 km s⁻¹.
- Fig. 5.— Spectrum in the region of line splitting showing the H α and two [N II] lines. The spectrum is an average over 5 pixels (3.4" or 150 pc) at R=4 kpc on the SE side.
- Fig. 6.— Dependence of line ratios on slit position for the perpendicular slit. In each panel, the normalized H α surface brightness is plotted. At $z \lesssim 1$ kpc, dust absorption causes an apparent local minimum in the H α emission. The line ratios plotted are (a) [S II] $\lambda 6716/\text{H}\alpha$, (b) [N II] $\lambda 6583/\text{H}\alpha$, (c) [O I] $\lambda 6300/\text{H}\alpha$, (d) [S II] $\lambda 6716/[\text{N II}]$ $\lambda 6583$, and (e) [O III] $\lambda 5007/\text{H}\beta$.
- Fig. 7.— The dependence of (a) [N II] $\lambda 6583/\text{H}\alpha$ (filled circles), [S II] $\lambda 6716/\text{H}\alpha$ (open circles), [S II] $\lambda 6716/[\text{N II}] \lambda 6583$ (crosses), and (b) $3\times[\text{O I}] \lambda 6300/\text{H}\alpha$ (filled circles) and [O III] $\lambda 5007/\text{H}\beta$ (open circles) on $\text{H}\alpha$ surface brightness. Note that the [O I]/ $\text{H}\alpha$ line ratio values and error bars have been multiplied by 3.
- Fig. 8.— Diagnostic diagrams of logarithmic line ratios: (a) [O III]/H β vs. [N II]/H α , (b) [O III]/H β vs. [S II]/H α , (c) [O I]/H α vs. [N II]/H α , (d) [O I]/H α vs. [S II]/H α , and (e) [S II]/H α vs. [N II]/H α . The curves are predictions from the radiation-bounded dilute photo-ionization model (called PM in the text) from S94. Open circles indicate values of the logarithm of the ionization parameter, log U=-2.3, -2.7, -3.0, -3.3, -3.7, -4.0, -4.3, and -4.7. In (e), the sequence begins at log U=-2.7.
- Fig. 9.— Diagnostic diagrams of logarithmic line ratios: (a) [O III]/H β vs. [N II]/H α , (b) [O III]/H β vs. [S II]/H α , (c) [O I]/H α vs. [N II]/H α , (d) [O I]/H α vs. [S II]/H α , and (e) [S II]/H α vs. [N II]/H α . The curves are predictions from a matter-bounded dilute photo-ionization model (called PM in the

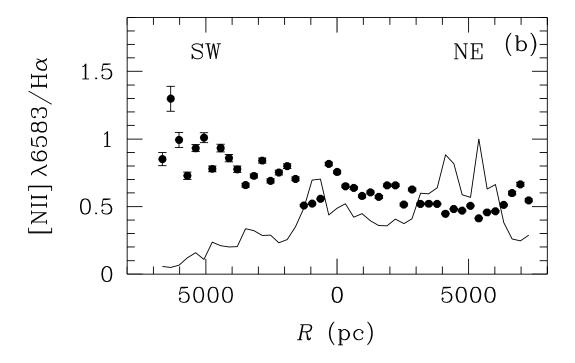
text) from S94. Small open circles indicate values of the logarithm of the ionization parameter, $\log U = -3.3, -3.7, -4.0, -4.3, -4.7$ and -5.0, although the first value may differ between plots. The triangle, square, and pentagon represent, respectively, line ratios from the standard-abundance 90 km s⁻¹ and 100 km s⁻¹ shock models and the depleted-abundance 100 km s⁻¹ shock model of SM. The large open circles joined by dashed lines represent the composite photo-ionization/shock-ionization model. These circles represent values of the ionization parameter of the photo-ionized component, $\log U = -4.0, -4.3, -4.7$ and -5.0. The fraction of emission from the 90 km s⁻¹ shock ranges from 7% at the left end of the sequence to 30% at the right end. Note that the lowest appropriate value of $\log U$ for a given line ratio depends on the maximum height above the plane at which it has been detected. See text for the best values of $\log U$ at various heights.

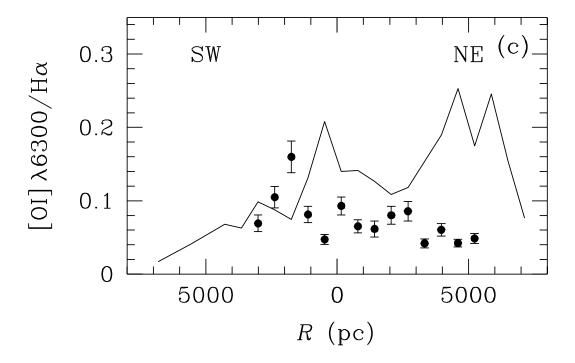
Fig. 10.— Diagnostic diagrams as in Figure 9 except that the composite photo-ionization/turbulent mixing layer model is now plotted as the large open circles joined by dashed lines. These circles represent values of the ionization parameter of the photo-ionized component, $\log U = -4.1$, -4.3, -4.7 and -5.0. The fraction of emission from the TML model ranges from 3% at the left end of the sequence to 15% at the right end. Note that the lowest appropriate value of $\log U$ for a given line ratio depends on the maximum height above the plane at which it has been detected. See text for the best values of $\log U$ at various heights. The triangle represents line ratios from a pure TML model.

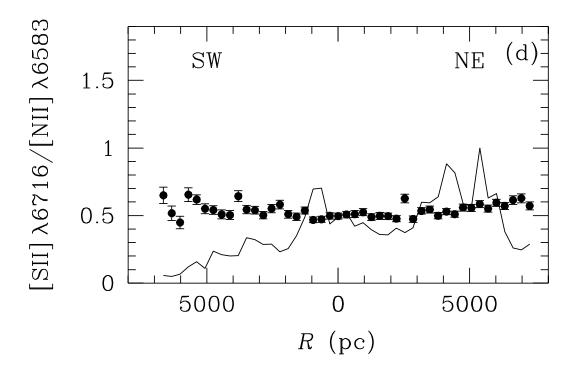


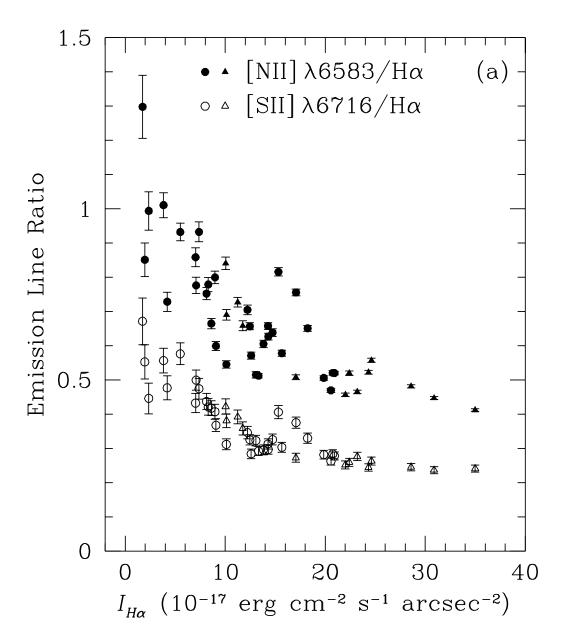


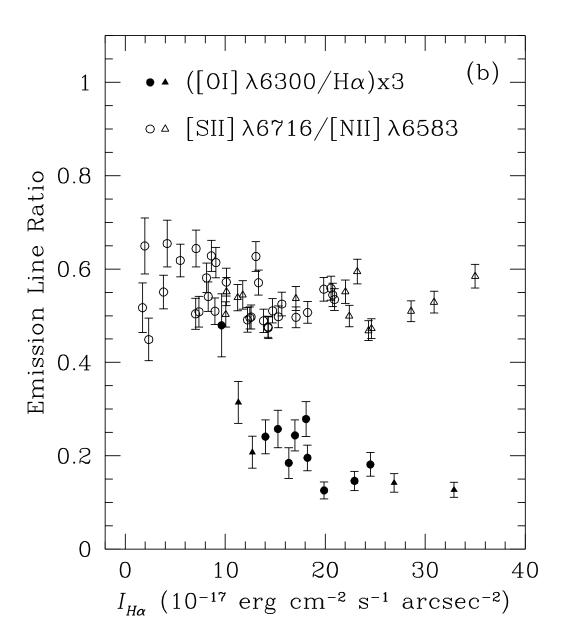


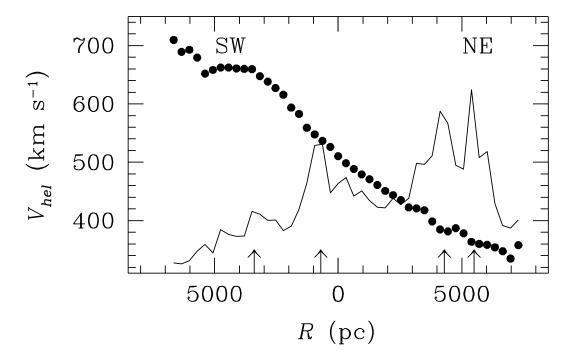


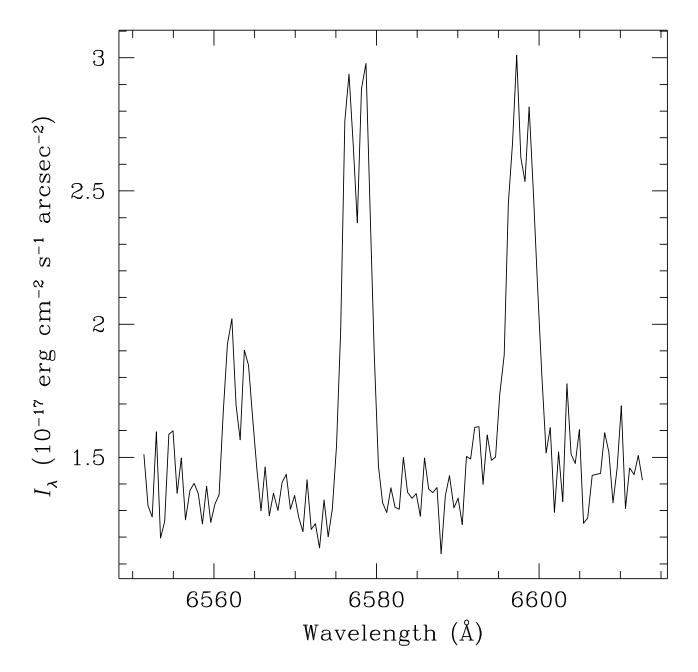


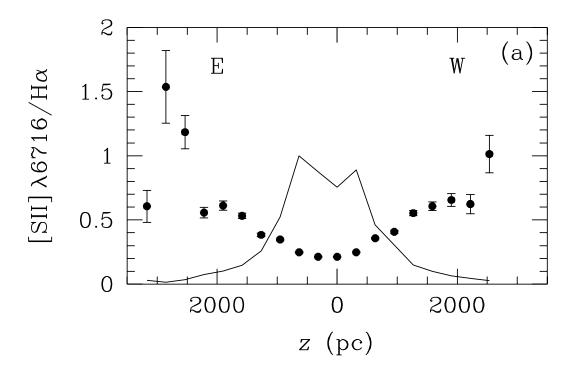


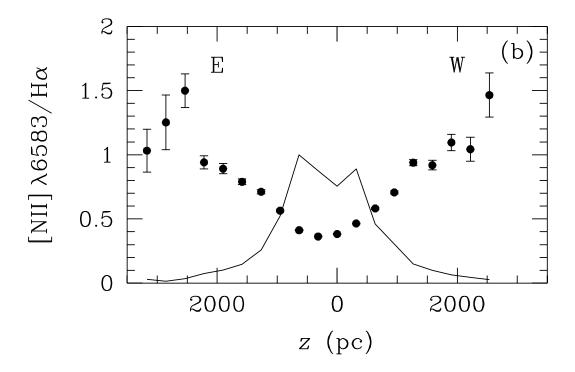


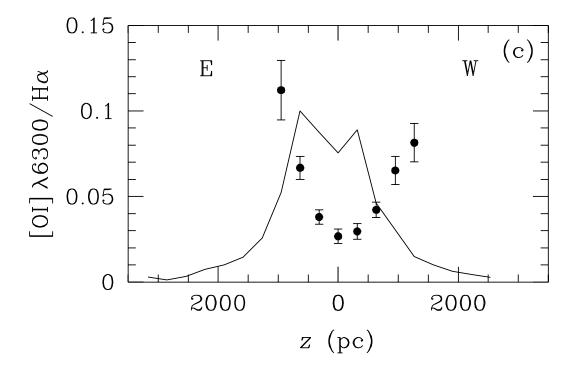


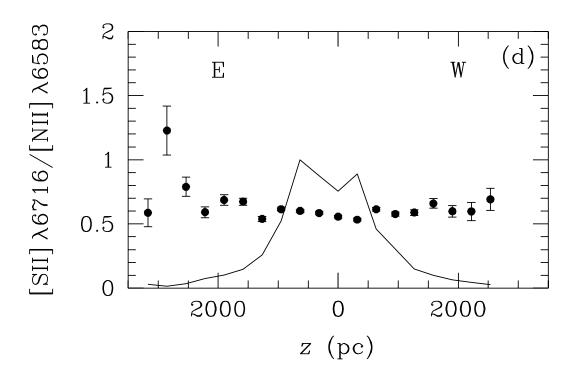


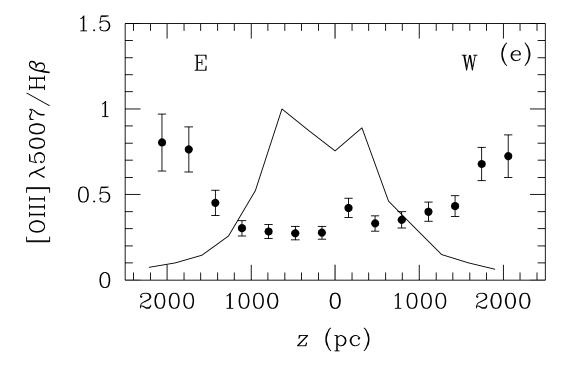


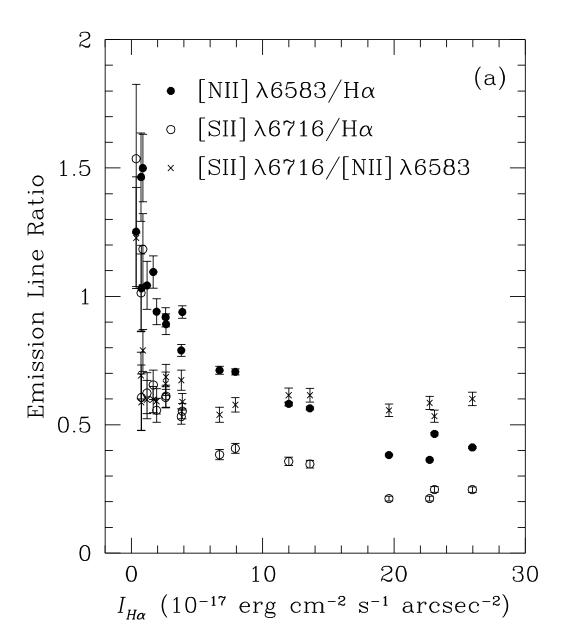


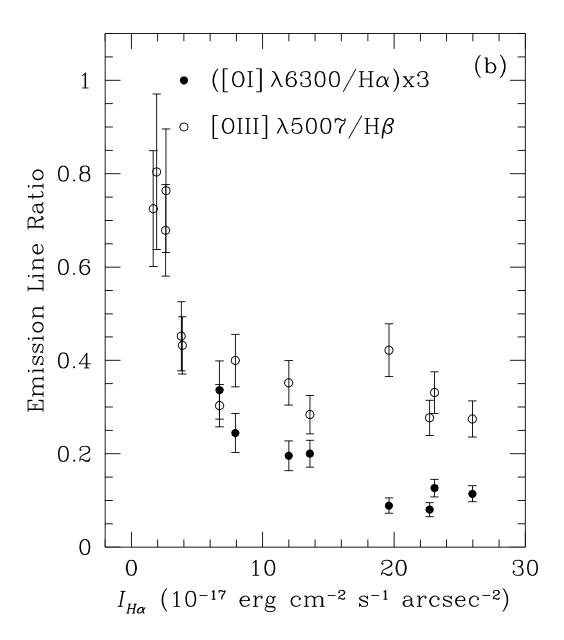


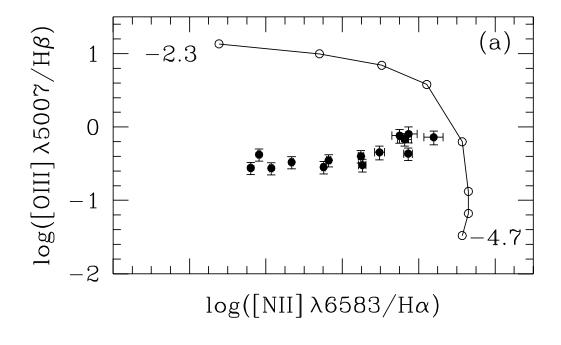


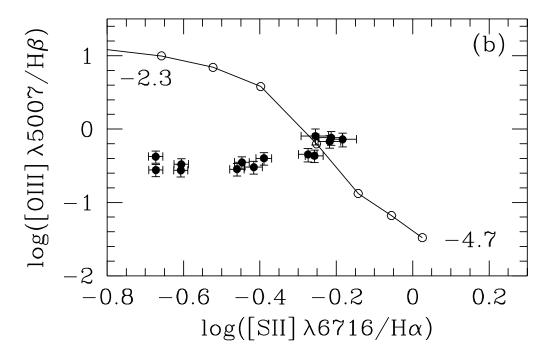


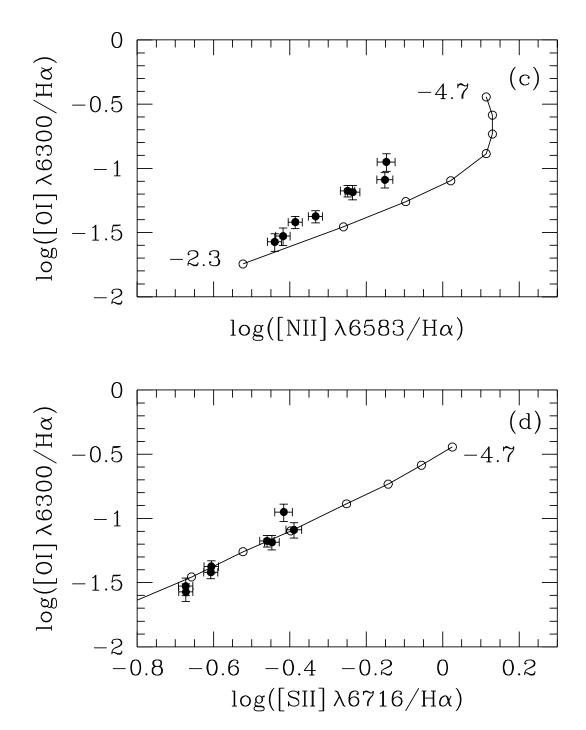


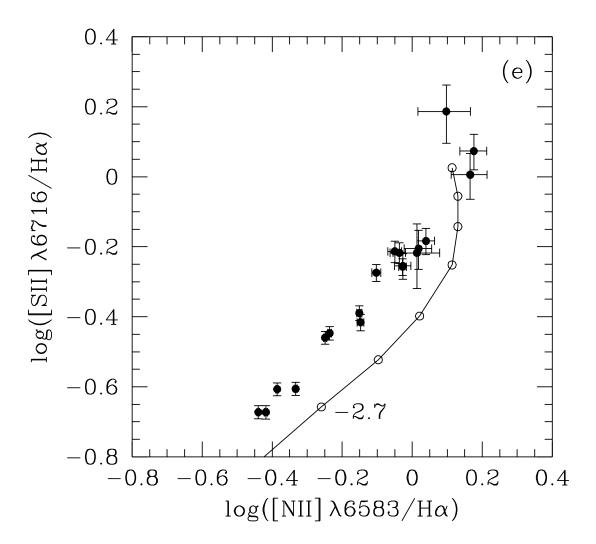


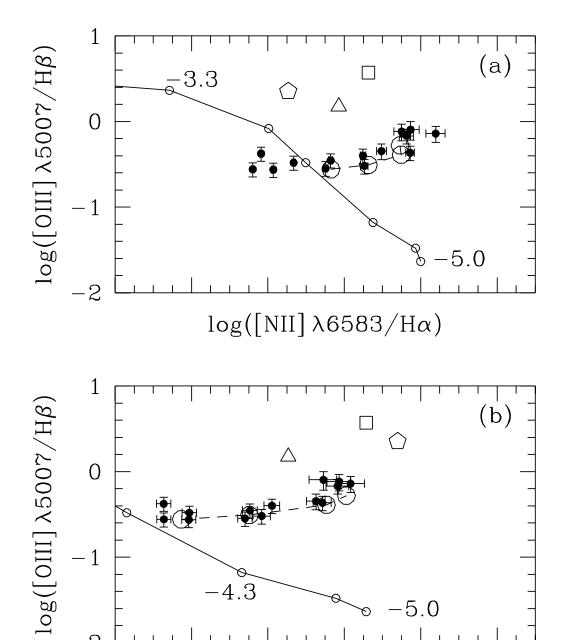












-2 LL -0.8

-0.6

-0.4

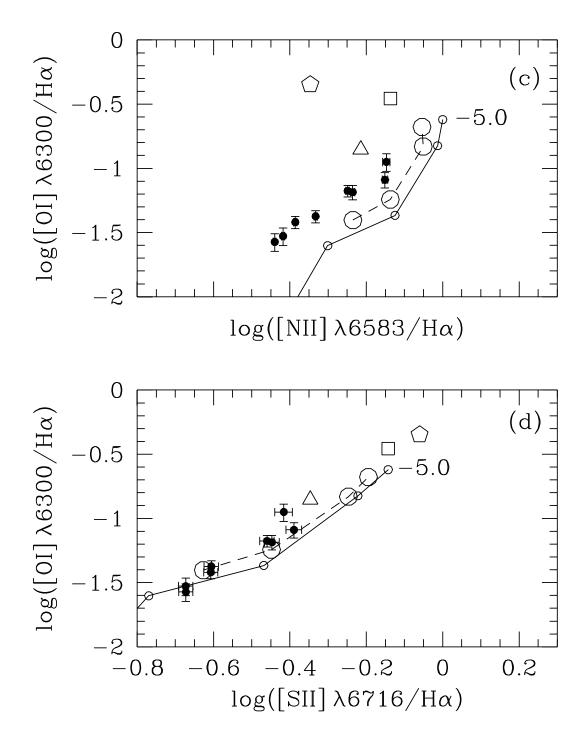
-5.0

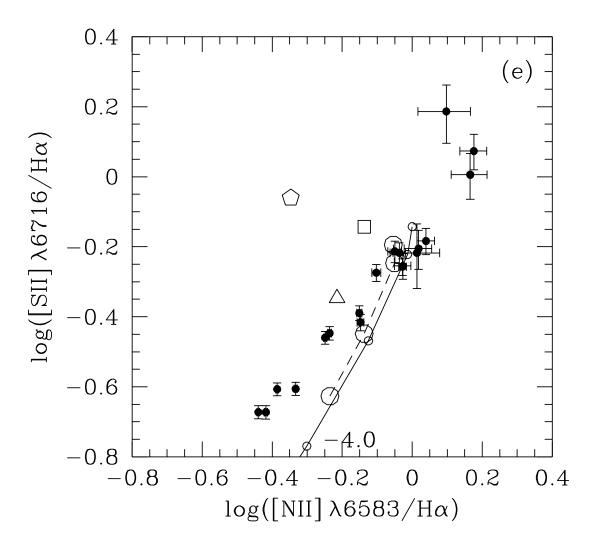
0

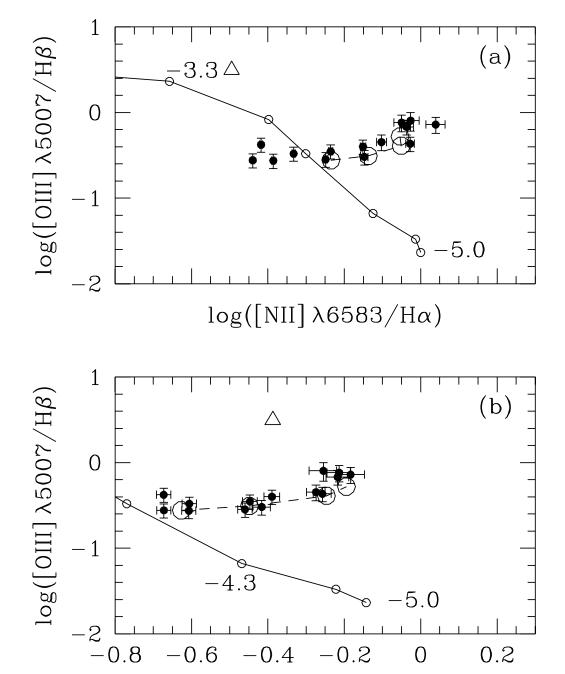
0.2

-0.2

 $\log([SII] \lambda 6716/H\alpha)$







 $\log([SII] \lambda 6716/H\alpha)$

